Suppression of synchronous resonance for VSGs

Yang, Dongsheng; Wu, Heng; Wang, Xiongfei; Blaabjerg, Frede

Published in:
The Journal of Engineering

DOI (link to publication from Publisher):
10.1049/joe.2017.0792

Publication date:
2017

Document Version
Publisher's PDF, also known as Version of record

The 6th International Conference on Renewable Power Generation (RPG)

19–20 October 2017

Suppression of synchronous resonance for VSGs

Dongsheng Yang, Heng Wu, Xiongfei Wang, Frede Blaabjerg

Department of Energy Technology, Aalborg University, Aalborg 9220, Denmark
E-mail: doy@et.aau.dk

Published in *The Journal of Engineering*; Received on 12th October 2017; Accepted on 1st November 2017

Abstract: The virtual synchronous generator (VSG) is an attractive interfacing technique for high-penetration renewable generation. By incorporating the inertia control, the grid-connected voltage-source converter can behave in a similar way with the SGs, which is helpful to enhance the stability of the power system. However, it is reported that the synchronous frequency resonance (SFR) can be aroused in the VSG due to the resonance peaks in the power control loops at the fundamental frequency. By modelling the power control loop in the *dq* domain, the mechanism underlying the SFR is studied. It reveals the frequency shift of the grid impedance in *dq* frame is the origin of SFR. Moreover, the phase-amplitude cross-regulation scheme is proposed to suppress the SFR. In this way, the resonance peaks in the power control loops are completely removed, and the coupling effects between the active power and reactive power loops are also eliminated. Therefore, superior power control performances can be achieved. Simulation results verify the effectiveness of the theoretical analysis and both dynamic performance and stability of the power loops are greatly improved by the proposed cross-regulation scheme.

1 Introduction

Over the past decade, renewable energy-based distributed power generations have been continuously integrated into power grids [1]. The grid-connected voltage-source converters (VSCs) are widely used as the interface in the renewable power plants and distribution networks. The dynamic interactions among the VSCs and the grid tend to bring in various resonance and stability issues, challenging stable operations of modern power systems [2].

The current-controlled scheme is dominated control method for grid-connected VSCs, which regulates the instantaneous active power and reactive power through the fast inner current control loop [3]. To synchronise with the grid, a phase-locked loop (PLL) is used to obtain the accurate phase angle of the voltage at the point of common coupling (PCC). However, under the weak grid condition, the PCC voltage is affected by the injection of active and reactive powers. Thus, subsynchronous resonance (SSR) and super-SR can be aroused due to the PLL dynamics [4–7]. Moreover, controlled as the current source, the VSC is incapable of providing the independent voltage support for the loads [8]. These issues impede the further increase of the renewable penetration level.

To enhance the stability of the power system dominated by power electronics, the concept of virtual synchronous generators (VSGs) was proposed to control the grid-connected VSCs to emulate the SGs including the inertial characteristic [9–12]. Instead of using PLL, VSG regulates its active power by adjusting the phase angle of the terminal voltage, while regulates its reactive power by varying its voltage magnitude, thus the negative impact of PLL on power stability can be eliminated. However, several investigations have shown that a resonant peak at the fundamental frequency in the power control loops of VSG tends to trigger SR [13–15] in contrast to SSR and super-SR. To address the SR, the virtual resistance can be implemented by control and inserted into line impedance, so that the SR can be retrained without introducing power loss [13]. However, this damping method will equivalently increase the *R/X* ratio of line impedance, which would inevitably make the coupling effects between the active and reactive powers more seriously.

In this paper, according to the complex power definition, the accurate power control model of VSG is derived in a straightforward way. Instead of using the virtual resistor to damp the SR peak, the phase-amplitude cross-regulation scheme is proposed for VSG, which can remove resonance peaks completely. Moreover, the coupling effects between the active and reactive power control loops are also greatly eliminated. In this way, the stability of VSG is greatly enhanced over the wideband frequency range and it is more flexible for VSG to choose power regulation parameters to achieve superior control performance.

2 Modelling of the power control loops for VSG

The topology and control block diagram of VSG is shown in Fig. 1. A three-phase voltage-source inverter is connected to the grid at the PCC through an inductor–capacitor filter, which consists of L_f and C_f. Z_g is the equivalent grid impedance at the PCC, which is modelled by a resistor r_g and a series inductor Lg. To mimic the key behaviour of the SG,, the damping and inertial controls are incorporated into the active power and reactive power regulations. D_p and D_q are damping coefficients of the active power and reactive power, respectively, and J and K_e are the rotating inertia and excitation coefficient. The output of the power regulations are used to adjust the phase θ and amplitude E of the terminal voltage $\boldsymbol{e}_{abc}$ with respect to the grid voltage $\boldsymbol{u}_{abc}$.

For better understanding, both the power calculation and the terminal voltage control are performed under the *dq* frame transformed by power constant constraint. In this way, the output instantaneous active and reactive powers of the VSG under *dq* frame can be expressed as [16]

$$P = e_d i_d + e_q i_q \tag{1}$$

$$Q = e_q i_d - e_d i_q \tag{2}$$

where e_d and e_q are the terminal voltages in the *dq* frame, the output currents in the *dq* frame, which can be rewritten in the form of

doi: 10.1049/joe.2017.0792

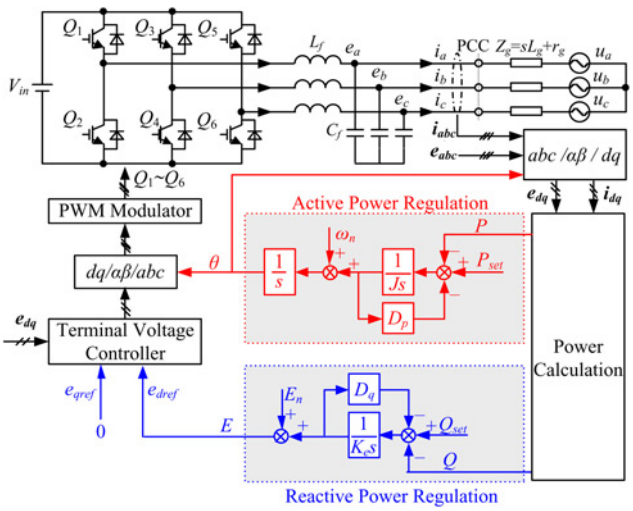

Fig. 1 *Topology and control scheme of VSG*

complex space vectors as

$$\boldsymbol{e}_{dq} = e_d + \mathrm{j}e_q \tag{3}$$

$$\boldsymbol{i}_{dq} = i_d + \mathrm{j}i_q \tag{4}$$

Therefore, the relationship between the complex power vector $\boldsymbol{S}$ and the complex vectors $\boldsymbol{e}_{dq}$, $\boldsymbol{i}_{dq}$ can be derived as

$$\begin{aligned}\boldsymbol{S} &= P + \mathrm{j}Q \\ &= (e_d i_d + e_q i_q) + \mathrm{j}(e_q i_d - e_d i_q) \\ &= (e_d + \mathrm{j}e_q)(i_d - \mathrm{j}i_q) \\ &= \boldsymbol{e}_{dq} \cdot \boldsymbol{i}_{dq}^{*}\end{aligned} \tag{5}$$

where * denotes the conjugation operation.

In VSG, the output current vector $\boldsymbol{i}_{dq}$ is indirectly controlled by adjusting terminal voltage vector $\boldsymbol{e}_{dq}$ with respect to the grid voltage vector $\boldsymbol{u}_{dq}$, i.e.

$$\boldsymbol{i}_{dq} = \frac{\boldsymbol{e}_{dq} - \boldsymbol{u}_{dq}}{\boldsymbol{Z}_{gdq}} \tag{6}$$

where $\boldsymbol{Z}_{gdq}$ is the grid impedance in the dq frame.

According to the frequency transformation between dq frame and $\alpha\beta$ frame [17], and considering $\boldsymbol{Z}_{g\alpha\beta} = sL_g + r_g$, the expression of $\boldsymbol{Z}_{gdq}$ can be derived as

$$\boldsymbol{Z}_{dq}(s) = \boldsymbol{Z}_{\alpha\beta}(s + j\omega_n) = sL_g + j\omega_n L_g + r_g \tag{7}$$

Moreover, since the control loop of terminal voltage has much faster dynamics than the power regulation, it is assumed that the terminal voltage $\boldsymbol{e}_{dq}$ can accurately follow its reference, with a leading phase $\Delta\theta$ with respect to $\boldsymbol{u}_{dq}$, i.e.:

$$\boldsymbol{e}_{dq} = E \cdot \mathrm{e}^{\mathrm{j}0} \tag{8}$$

$$\boldsymbol{u}_{dq} = U \cdot \mathrm{e}^{-\mathrm{j}\Delta\theta} \tag{9}$$

where the physical meanings of E and U are the root-mean-square (RMS) values of the line-line terminal voltage and grid voltage, respectively.

Substituting (6)–(9) into (5), yielding

$$\begin{aligned}\boldsymbol{S} &= \boldsymbol{e}_{dq} \cdot \left(\frac{\boldsymbol{e}_{dq} - \boldsymbol{u}_{dq}}{\boldsymbol{Z}_{gdq}}\right)^{*} = \frac{E^2 - EU \cdot \mathrm{e}^{\mathrm{j}\Delta\theta}}{sL_g + r_g - \mathrm{j}\omega_n L_g} \\ &\simeq \frac{E^2 - EU(1 + \mathrm{j}\Delta\theta)}{sL_g + r_g - \mathrm{j}\omega_n L_g} = \frac{E.\Delta E - \mathrm{j}EU \cdot \Delta\theta}{sL_g + r_g - \mathrm{j}\omega_n L_g}\end{aligned} \tag{10}$$

where $\Delta E = E - U$ denoting the difference between the VSG terminal voltage and grid voltage.

As a result, the output instantaneous active power and the reactive power of VSG can be rewritten as

$$\begin{aligned}P &= \mathrm{Re}(\boldsymbol{S}) \\ &= \underbrace{\frac{\omega_n L_g EU}{(sL_g + r_g)^2 + (\omega_n L_g)^2}}_{G_{\theta P}(S)} \cdot \Delta\theta + \underbrace{\frac{(sL_g + r_g)E}{(sL_g + r_g)^2 + (\omega_n L_g)^2}}_{G_{EP}(S)} \cdot \Delta E\end{aligned} \tag{11}$$

$$\begin{aligned}Q &= \mathrm{Im}(\boldsymbol{S}) \\ &= \underbrace{\frac{\omega_n L_g E}{(sL_g + r_g)^2 + (\omega_n L_g)^2}}_{G_{EQ}(S)} \cdot \Delta E + \underbrace{\frac{-(sL_g + r_g)EU}{(sL_g + r_g)^2 + (\omega_n L_g)^2}}_{G_{\theta Q}(S)} \cdot \Delta\theta\end{aligned} \tag{12}$$

Therefore, according to (11), (12) and Fig. 1, the control block diagram of power control loops can be given by Fig. 2.

3 Mechanism of synchronous frequency resonance (SFR) and power loop coupling

According to Fig. 2, the active power loop and reactive power loop are coupled with each other due to $G_{\theta Q}(s)$ and $G_{EP}(s)$. Moreover, all $G_{\theta P}(s)$, $G_{EQ}(s)$, $G_{\theta Q}(s)$ and $G_{EP}(s)$ contain a pair of conjugate poles, which can be expressed as

$$S_{1,2} = -r_g/L_g \pm \mathrm{j}\omega_n \tag{13}$$

When the passive damping in the grid impedance is weak, i.e. $R/(L\omega_n)$ ratio is low, the poles will move closer to the imaginary axis. As a result, the oscillation can be potentially triggered near the synchronous frequency ω_n, namely SFR. Fig. 3 gives the FRs of $G_{\theta P}(s)$, $G_{EQ}(s)$, $G_{\theta Q}(s)$ and $G_{EP}(s)$ when $R/(L\omega_n) = 1\%$. There are resonance peaks and $-180°$ phase jump at the synchronous frequency (50 Hz).

Referring to (10), it can be seen that if $\boldsymbol{Z}_{gdq}$ only contains real part $\boldsymbol{Z}_{gdq} = sL_g + r_g$, the complex power vector $\boldsymbol{S}$ can be simplified as

$$\boldsymbol{S} \simeq \frac{E}{sL_g + r_g} \cdot \Delta E - \frac{\mathrm{j}EU}{sL_g + r_g} \cdot \Delta\theta \tag{14}$$

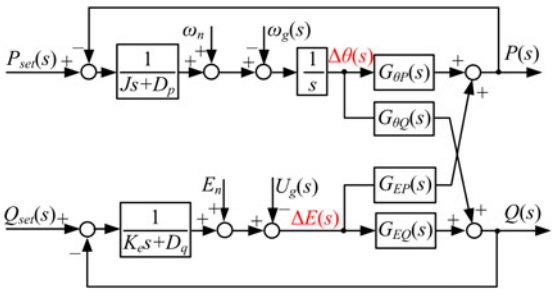

Fig. 2 *Control block diagram of power control loops*

doi: 10.1049/joe.2017.0792

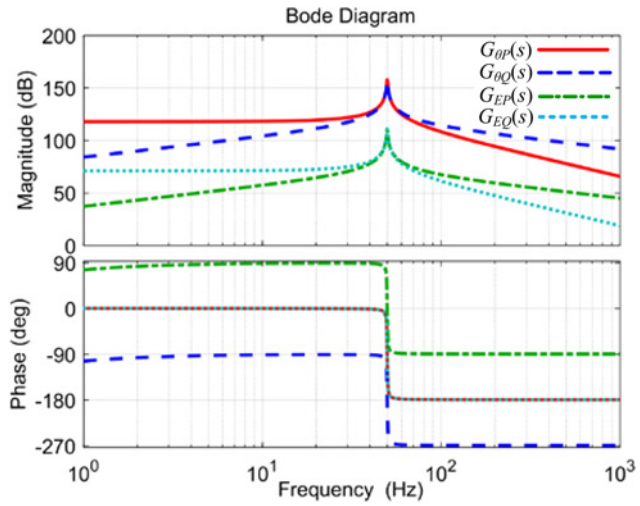

Fig. 3 *FRs of the control plant for power loops*

Then the active power (the real part of $\boldsymbol{S}$), can be regulated by ΔE, while the reactive power (the imaginary part of $\boldsymbol{S}$) can be regulated by $\Delta\theta$. On the other hand, if the $\boldsymbol{Z}_{gdq}$ only contains the imaginary part, i.e. $\boldsymbol{Z}_{g\alpha\beta}=\mathrm{j}\omega_n L_g$, the complex power vector $\boldsymbol{S}$ can be simplified as

$$\boldsymbol{S} \simeq \frac{EU}{\omega_n L_g}\cdot\Delta\theta + \frac{\mathrm{j}E}{\omega_n L_g}\cdot\Delta E \tag{15}$$

Then, the active power and reactive power can also be regulated independently by adjusting $\Delta\theta$ and ΔE, respectively.

For both of the two cases, the coupling effect between the power control loops does not exist. Moreover, no conjugate poles are generated. In this sense, both the coupling effects and the SFR hazard are resulted by the mixed real and imaginary parts of $\boldsymbol{Z}_{gdq}$. This characteristic is introduced by the frequency shift operation during the transformation from $\alpha\beta$ frame to dq frame.

Fig. 4 gives the FRs of $\boldsymbol{Z}_{g\alpha\beta}$ and $\boldsymbol{Z}_{gdq}$. Since the inductance tends to be zero for the dc component, therefore, $\boldsymbol{Z}_{g\alpha\beta}$ is approximated to the resistance of r_g near the zero frequency and an anti-resonance peak would be formed if rg is small. This anti-resonance peak would be moved to negative synchronous frequency $-\omega n$ for $\boldsymbol{Z}_{gdq}$. According to (10), the complex power vector $\boldsymbol{S}$ is proportion to the conjugation of grid admittance $1/\boldsymbol{Z}^*_{gdq}$, of which the FR is shown by the dotted line in Fig. 4. As a result, a resonance peak would be generated in the power loops at the positive synchronous frequency ωn.

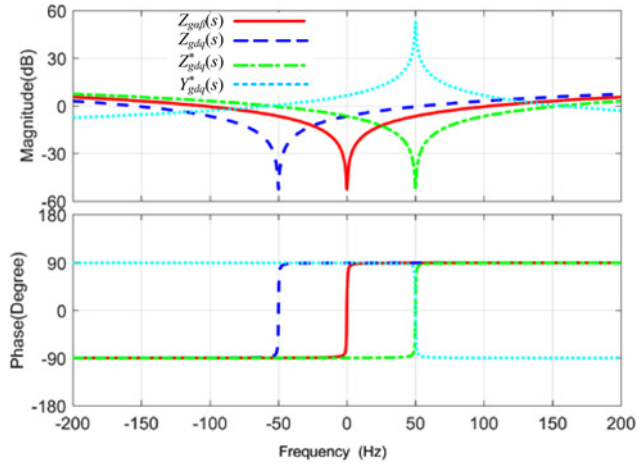

Fig. 4 *Frequency shift effect on the grid impedance in dq frame*

4 Suppression of SFR

A straightforward method to damp the SFR is to increase the R/L ratio, which can be implemented using the virtual resistor techniques [13]. However, this method can only tune the conjugate poles, as shown in (13), away from the imaginary axis instead of removing them. As a result, these poles may still impose significant impacts on the power control.

First, the active power and reactive power control are still coupled with each other, which make it difficult to tune the parameter of power regulation. Moreover, increasing R/L tends to make the coupling between active power and reactive power more severe, and multi-input–multi-output stability analysis should be performed to ensure the stability of the system [18]. Another major issue lies is

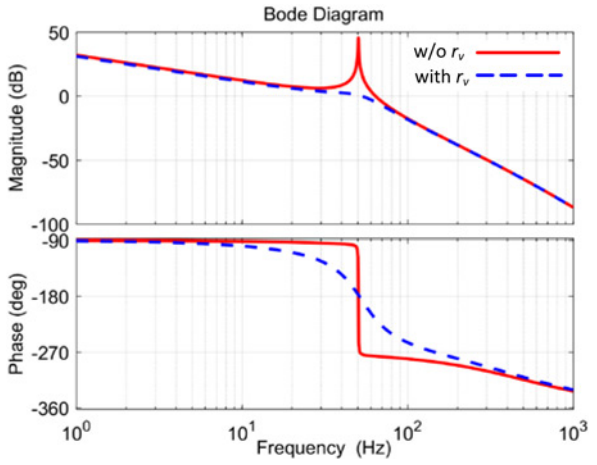

Fig. 5 *FR of active power control loop gain*

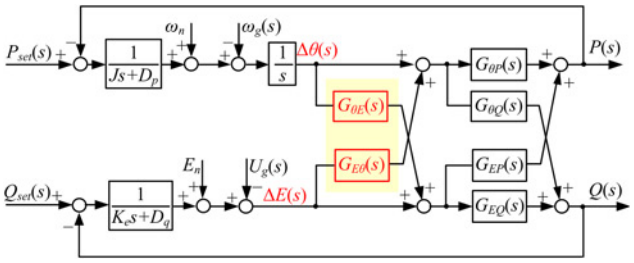

Fig. 6 *Phase-amplitude cross-regulation scheme*

Table 1 Main circuit parameters of VSG

Parameters	Value	Parameters	Value, pu
grid voltage U (L–L RMS)	400 V (1 pu)	filter inductor L_f	0.02
rated power S	10 kVA (1 pu)	filter capacitor C_f	0.01
fundamental frequency f_n	50 Hz	grid inductor L_g (short circuit ratio (SCR) = 3)	0.33
switching frequency f_s	10 kHz	grid resistor r_g	0.0033

Table 2 Control parameters of VSG

Parameters	Case I	Case II
inertia J	0.31	0.0031
excitation gain K_e	1.59	0.04
P damping coefficient D_p	127	3.18
Q damping coefficient D_q	100	2.5

doi: 10.1049/joe.2017.0792

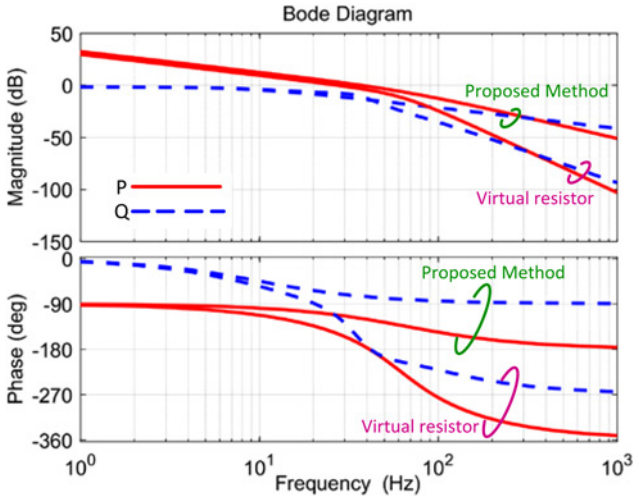

Fig. 7 *Bode diagram of power loop gains with parameters of Case I*

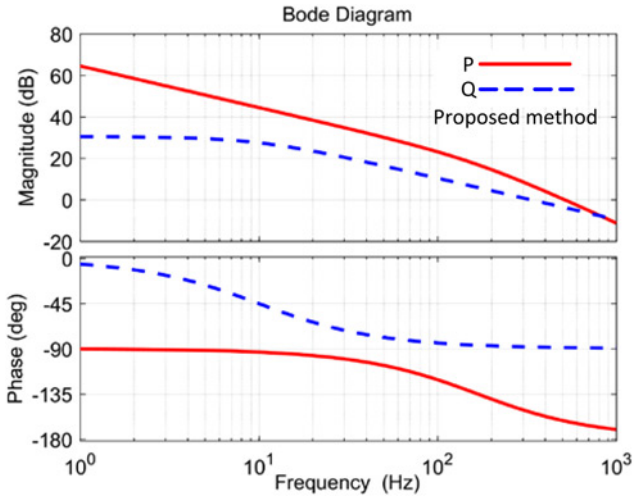

Fig. 8 *Bode diagram of power loop gains with parameters of Case II*

that this pair of poles creates a −180° phase lag, which can impose a great limitation on the power control bandwidth. Fig. 5 shows the FR of active power control loop gain. Considering the inertia J and the pure integrator $1/s$ in the active power loop, the phase lag introduced by the conjugate poles make the phase angle of the active power loop approach to −360° after the synchronous frequency. Therefore, even when the resonance peak is damped by the virtual resistor rv, it is still difficult to increase the control bandwidth beyond the synchronous frequency.

Therefore, it is desirable to remove the conjugate poles to decouple the power controls and free the power bandwidth limitation. In this paper, the phase-amplitude cross-regulation scheme is proposed to achieve this target, as shown in Fig. 6, where the transfer functions of coupling terms are given by

$$G_{\theta E}(s) = \frac{U}{\omega_n}\left(s + \frac{r_g}{L_g}\right) \tag{16}$$

$$G_{E\theta}(s) = -\frac{1}{U\omega_n}\left(s + \frac{r_g}{L_g}\right) \tag{17}$$

In this way, the equivalent control plant of power loop can be derived as

$$G'_{\theta P}(s) = G_{\theta P}(s) + G_{\theta E}(s)\cdot G_{EP}(s) = \frac{EU}{\omega_n L_g} \tag{18}$$

$$G'_{\theta Q}(s) = G_{\theta Q}(s) + G_{\theta E}(s)\cdot G_{EQ}(s) = 0 \tag{19}$$

$$G'_{EP}(s) = G_{EP}(s) + G_{E\theta}(s)\cdot G_{\theta P}(s) = 0 \tag{20}$$

$$G'_{EQ}(s) = G_{EQ}(s) + G_{U\theta}(s)\cdot G_{\theta Q}(s) = \frac{E}{\omega_n L_g} \tag{21}$$

As a result, both the conjugate poles and the power loop coupling can be removed.

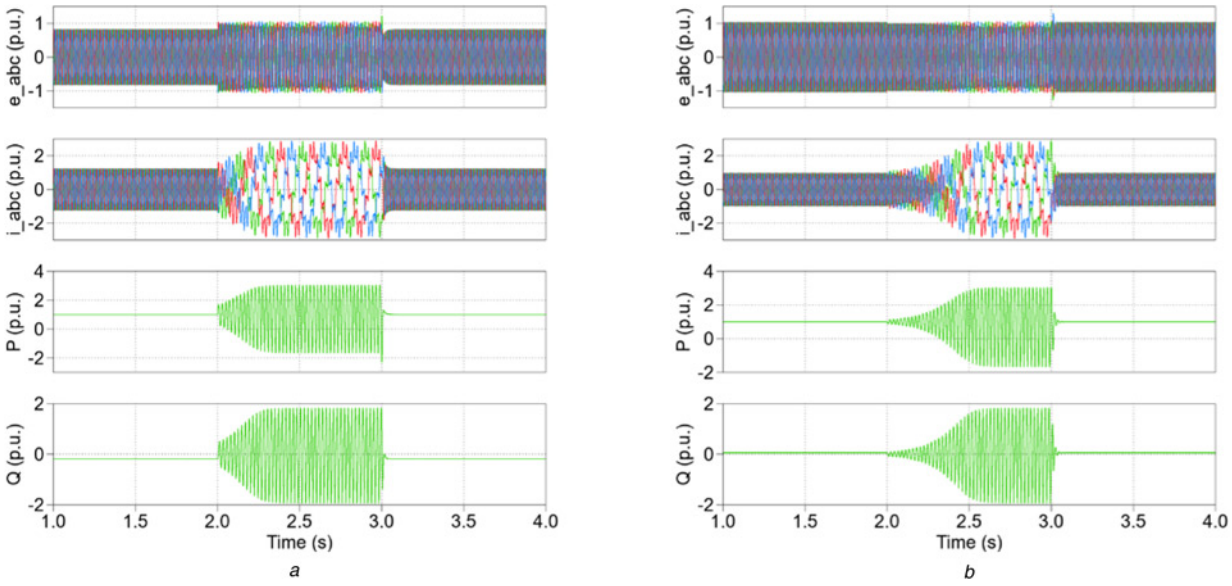

Fig. 9 *Suppression of the SFR*
a Using virtual resistor
b Using proposed method

doi: 10.1049/joe.2017.0792

5 Simulation verification

The parameters of the VSG is shown in Tables 1 and 2. Figs. 7 and 8 show Bode diagrams of power loop gains with parameters of Case I and Case II in Table 2, respectively.

5.1 Suppression of the SFR

To verify the suppression of the SFR, both the virtual resistor and the proposed phase-amplitude cross-regulation are disabled at $t = 2.0$ s, and then are enabled again at $t = 3.0$ s, as shown in Fig. 9. An obvious SFR is generated without damping control. Moreover, both the virtual resistor and proposed method can effectively suppress the SFR.

5.2 Transient stability

Fig. 10 presents the dynamic waveforms with the step change of active power reference using control parameters of Case I.

Using the virtual resistor method, a transient instability is triggered due to the step change of the active power, while this transient instability is eliminated by the proposed phase-magnitude cross-regulation scheme. It is similar for the step change of reactive power reference, which is not presented here due to the page limit.

5.3 Control bandwidth breakthrough

Fig. 11 presents the dynamic waveforms with the step change of power references using control parameters of Case II. The settling time of the active power control can be much less than the

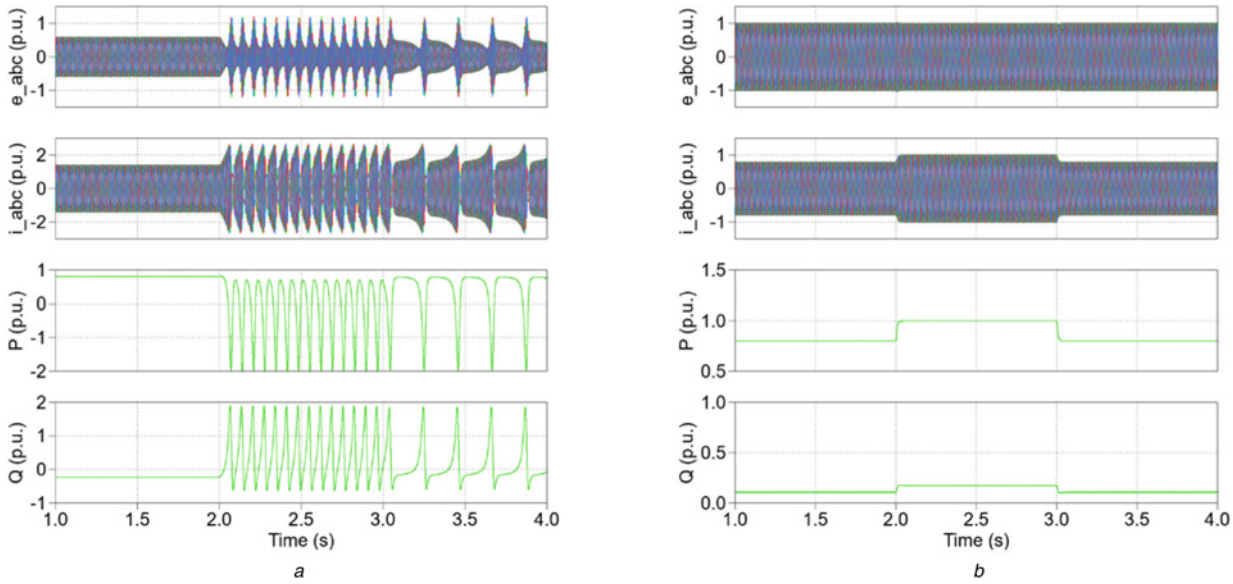

Fig. 10 *Dynamic waveforms with a step change of active power reference*
a Using virtual resistor
b Using proposed method

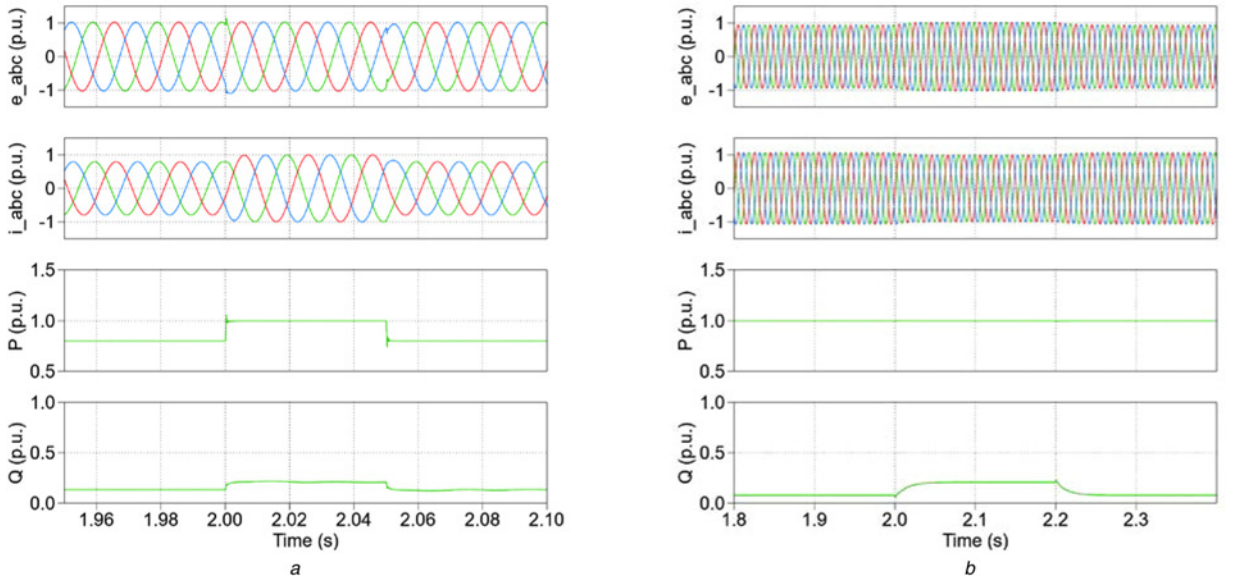

Fig. 11 *Improved dynamic waveforms with a step change of*
a Active power reference
b Reactive power reference

doi: 10.1049/joe.2017.0792

fundamental period. Therefore, it verifies that the control bandwidth of the power control can be increased above the synchronous frequency with the proposed method.

6 Conclusion

By modelling of the power control loop of VSG, the mechanism underlying the SFR is investigated. It reveals the frequency shift of the grid impedance in *dq* frame is the very origin of SFR and the coupling effects between the active and reactive power loops. Thus, the phase-amplitude cross-regulation scheme is proposed to suppress the SFR. In this way, the resonance peaks in the power control loops are completely removed, and the coupling effects between the active power and reactive power loops are also eliminated. Therefore, the stability of VSG is greatly enhanced over the wideband frequency range, and superior power control performances can be achieved.

7 References

[1] Blaabjerg F., Teodorescu R., Liserre M., *ET AL.*: 'Overview of control and grid synchronization for distributed power generation systems', *IEEE Trans. Ind. Electron.*, 2006, **53**, pp. 1398–1409

[2] Wang X., Blaabjerg F., Wu W.: 'Modeling and analysis of harmonic stability in an AC power-electronics-based power system', *IEEE Trans. Power Electron.*, 2014, **29**, pp. 6421–6432

[3] Kazmierkowski M.P., Malesani L.: 'Current control techniques for three-phase voltage-source PWM converters: a survey', *IEEE Trans. Ind. Electron.*, 1998, **45**, pp. 691–703

[4] Harnefors L., Bongiornos M., Lundberg S.: 'Input-admittance calculation and shaping for controlled voltage-source converters', *IEEE Trans. Ind. Electron.*, 2007, **54**, pp. 3323–3334

[5] Messo T., Jokipii J., Makinen A., *ET AL.*: 'Modeling the grid synchronization induced negative-resistor-like behavior in the output impedance of a three-phase photovoltaic inverter'. Proc. IEEE Fourth Int. Symp. Power Electronics for Distributed Generations System, 2013, pp. 1–8

[6] Bo W., Dong D., Boroyevich D., *ET AL.*: 'Impedance-based analysis of grid-synchronization stability for three-phase paralleled converters', *IEEE Trans. Power Electron.*, 2016, **31**, pp. 26–38

[7] Zhou J., Gole A.: 'VSC transmission limitations imposed by AC system strength and AC impedance characteristics'. Proc. Tenth IET Int. Conf. AC and DC Power Transmission (ACDC), 2012, pp. 1–6

[8] Wu H., Ruan X., Yang D., *ET AL.*: 'Small-signal modeling and parameters design for virtual synchronous generators', *IEEE Trans. Ind. Electron.*, 2016, **63**, pp. 4292–4303

[9] Loix T.: 'Participation of inverter-connected distributed energy resources in grid voltage control'. PhD dissertation, Katholieke Universiteit Leuven, Leuven, 2011

[10] Beck H.-P., Hesse R.: 'Virtual synchronous machine'. Proc. Ninth Int. Conf. Electrical Power Quality and Utilisation, 2007, pp. 1–6

[11] Chen Y., Hesse R., Turschner D., *ET AL.*: 'Improving the grid power quality using virtual synchronous machines'. Proc. Power Engineering, Energy and Electrical Drives, 2011, pp. 1–6

[12] Zhong Q.-C., Weiss G.: 'Synchronverters: inverters that mimic synchronous generators', *IEEE Trans. Ind. Electron*, 2011, **58**, pp. 1259–1267

[13] Wang J., Wang Y., Gu Y., *ET AL.*: 'Synchronous frequency resonance of virtual synchronous generators and damping control'. Proc. Ninth Int. Conf. Power Electronics – ECCE Asia, 2015, pp. 1011–1016

[14] Zhang L., Nee H.P., Harnefors L.: 'Analysis of stability limitations of a VSC-HVDC link using power synchronization control', *IEEE Trans. Power Syst.*, 2011, **26**, pp. 1326–1337

[15] Zhang L., Harnefors L., Nee H.-P.: 'Power-synchronization control of grid-connected voltage-source converters', *IEEE Trans. Power Syst.*, 2010, **25**, pp. 809–820

[16] Akagi H., Watanabe E., Aredes M.: 'Instantaneous power theory and applications to power conditioning' (IEEE Press, NJ, 2007)

[17] Wang X., Harnefors L., Blaabjerg F.: 'A unified impedance model of grid-connected voltage-source converters', *IEEE Trans. Power Electron.*, 2018, **33**, pp. 1775–1787

[18] MacFarlane A.G.J., Postlethwaite I.: 'The generalized Nyquist stability criterion and multivariable root loci', *Int. J. Control*, 1977, **25**, pp. 81–127

doi: 10.1049/joe.2017.0792